

the in-plane mobility of the charge carriers would determine the device characteristics rather than the mobility perpendicular to the molecular planes, as in the case of single crystal cells. At optimum doping ($p \approx 10^{15} \text{ cm}^{-3}$) the anisotropy is of the order of 10^2 or 10^3 .

To enhance the open-circuit voltage we have used other low-work-function metals (like magnesium and calcium) as back contacts and found an enhancement of V_{oc} by up to 250 mV resulting in a maximum V_{oc} of 1,200 mV. At this point, the quality of these contacts needs further work to reduce losses caused by a low shunt resistance. Initial studies of device stability indicate no degradation during the first hours of operation. However, after 100 hours a loss in efficiency of approximately 10% is observed, which we may ascribe to interaction of iodine or bromine and aluminium at the back contact. In a first step to improve the long-term stability of these photovoltaic devices, dopants will have to be found that do not interact with the back-contact material. Then the intrinsic stability of the doped pentacene against photo-induced degradation will need to be studied.

The present results demonstrate that respectable photovoltaic performance can be achieved in a simply doped Schottky-diode structure based on organic semiconductors. Furthermore, the use of thin films, where thickness, conductivity, and doping ratio can be optimized, or the combination of doped pentacene with a suitable n-type material in a two-layer device^{19–21} show potentially even higher efficiencies. These first research results and progress in polymeric devices might open new perspectives for efficient 'plastic' solar cells. □

Methods

Crystal growth and doping

Pentacene single crystals are grown by horizontal physical vapour transport in a stream of hydrogen. The volatilization zone is heated to approximately 300 °C and the growth zone is kept at 200–280 °C. Trap and dopant densities as low as 10^{13} and 10^{11} cm^{-3} were measured using space-charge-limited current measurements. Iodine or bromine doping was performed by immersing the crystals into a solution of iodine or bromine in acetonitrile. The dopant density is adjusted by the iodine or bromine concentration of the solution.

Device fabrication

An approximately 300 nm thick, transparent ITO window layer was deposited onto a freshly cleaved (about 1 μm thick), doped single crystal by radio frequency magnetron sputtering (Leybold Z400 sputtering system). The typical conductivity of this layer was about 2000 S cm^{-1} . In addition a silver-contact finger was deposited onto the window layer in order to reduce series resistance losses. The Schottky contact (Al/Mg, 100 nm thick) was thermally evaporated. Typical cell areas are in the range 2–5 mm^2 .

Current–voltage characteristics

Current–voltage curves are measured in air at room temperature using a Keithley 238 Source-Measure-Unit. A commercial solar simulator is used as illumination source (Steuernagel, solar constant 575). Its intensity is adjusted using a calibrated and certified GaAs solar cell (ISE Institute für Solare Energieforschung, Freiburg). The current density is not numerically adjusted for the spectral mismatch between GaAs and doped pentacene.

Received 1 June; accepted 25 November 1999.

- Halls, J. J. M. *et al.* Efficient photodiodes from interpenetrating polymer networks. *Nature* **376**, 498–500 (1995).
- Yu, G., Gao, J., Hummelen, J. C., Wudl, F. & Heeger, A. J. Polymer photovoltaic cells: Enhanced efficiencies via a network of internal donor-acceptor heterojunctions. *Science* **270**, 1789–1791 (1995).
- Granström, M. *et al.* Laminated fabrication of polymeric photovoltaic diodes. *Nature* **395**, 257–260 (1998).
- Bach, U. *et al.* Solid-state dye-sensitized mesoporous TiO_2 solar cells with high photon-to-electron conversion efficiencies. *Nature* **395**, 583–585 (1998).
- Chamberlain, G. A., Cooney, P. J. & Dennison, S. Photovoltaic properties of merocyanine solid-state photocells. *Nature* **289**, 45–47 (1981).
- Lin, Y.-Y., Gundlach, D. J., Nelson, S. F. & Jackson, T. N. Pentacene-based organic thin-film transistors. *IEEE Trans. Electr. Dev.* **44**, 1325–1331 (1997).
- Nelson, S. F., Lin, Y.-Y., Gundlach, D. J. & Jackson, T. N. Temperature-independent transport in high-mobility pentacene transistors. *Appl. Phys. Lett.* **72**, 1854–1856 (1998).
- Dimitrakopoulos, C. D., Purushothaman, S., Kymissis, J., Callegari, A. & Shaw, J. M. Low voltage organic transistors on plastic comprising high dielectric constant gate insulators. *Science* **283**, 822–824 (1999).
- Signerski, R., Jarosz, G. & Godlewski, J. Photoelectric properties of heterojunctions formed from di-(pyridyl)-perylene-tetracarboxylic diimide and copper phthalocyanine or pentacene. *Synth. Met.* **94**, 135–137 (1998).

- Videlot, C., Fichou, D. & Garnier, F. Photovoltaic cells based on organic semiconductors. *J. Chim. Phys.* **95**, 1335–1338 (1998).
- Laudise, R. A., Kloc, Ch., Simpkins, P. G. & Siegrist, T. Physical vapor growth of organic semiconductors. *J. Cryst. Growth* **187**, 449–454 (1998).
- Mimikata, T., Imai, H., Ozaki, M. & Saco, K. Structural studies on highly ordered and highly conductive thin films of pentacene. *J. Appl. Phys.* **72**, 5220–5225 (1992).
- Schön, J. H., Kloc, Ch., Laudise, R. A. & Batlogg, B. Electrical properties of single crystals of rigid rodlike conjugate molecules. *Phys. Rev. B* **58**, 12952–12957 (1998).
- Minakata, T., Nagoya, I. & Ozaki, M. Highly ordered and conducting thin films of pentacene doped with iodine vapor. *J. Appl. Phys.* **69**, 7354–7356 (1991).
- Hovel, H. J. *Semiconductors and Semimetals* Vol. 11, *Solar Cells* 71–92 (Academic, New York, 1975).
- Karl, N. in *Semiconductors* (eds Madelung, O., Schulz, M. & Weiss, H.) Subvolume 17i, 106–218 (Landolt-Börnstein, New Series Vol. 17, Springer-Verlag, Berlin, 1985).
- Chamberlain, G. A. Depletion layer studies and carrier photogeneration in doped merocyanine photovoltaic cells. *J. Appl. Phys.* **53**, 6262–6269 (1982).
- Videlot, C. & Fichou, D. Influence of molecular orientation on the photovoltaic properties of octithiophene. *Synth. Met.* **102**, 885–888 (1999).
- Tang, C. W. Two-layer organic photovoltaic cell. *Appl. Phys. Lett.* **48**, 183–185 (1986).
- Wöhrl, D. *et al.* Investigations of n/p junction photovoltaic cells of perylene-tetracarboxylic acid diimides and phthalocyanines. *J. Mater. Chem.* **5**, 1819–1829 (1995).
- Wöhrl, D. & Meissner, D. Organic solar cells. *Adv. Mater.* **3**, 129–138 (1991).

Acknowledgements

We thank E. Chandross, Z. Bao, H. Katz and A. Dodabalapur for helpful discussions. J.H.S. gratefully acknowledges financial support by the 'Deutsche Forschungsgemeinschaft'.

Correspondence and requests for materials should be addressed to J.H.S. (e-mail: hendrik@lucent.com).

Rainfall and drought in equatorial east Africa during the past 1,100 years

Dirk Verschuren*†, Kathleen R. Laird‡ & Brian F. Cumming‡

*Limnological Research Center, University of Minnesota, Minneapolis, Minnesota 55455, USA

†Department of Biology, University of Gent, Ledeganckstraat 35, B-9000 Gent, Belgium

‡Paleoecological Environmental Assessment and Research Laboratory, Department of Biology, Queen's University, Kingston, Ontario K7L 3N6, Canada

Knowledge of natural long-term rainfall variability is essential for water-resource and land-use management in sub-humid regions of the world. In tropical Africa, data relevant to determining this variability are scarce because of the lack of long instrumental climate records and the limited potential of standard high-resolution proxy records such as tree rings and ice cores^{1–3}. Here we present a decade-scale reconstruction of rainfall and drought in equatorial east Africa over the past 1,100 years, based on lake-level and salinity fluctuations of Lake Naivasha (Kenya) inferred from three different palaeolimnological proxies: sediment stratigraphy and the species compositions of fossil diatom and midge assemblages. Our data indicate that, over the past millennium, equatorial east Africa has alternated between contrasting climate conditions, with significantly drier climate than today during the 'Medieval Warm Period' (~AD 1000–1270) and a relatively wet climate during the 'Little Ice Age' (~AD 1270–1850) which was interrupted by three prolonged dry episodes. We also find strong chronological links between the reconstructed history of natural long-term rainfall variation and the pre-colonial cultural history of east Africa⁴, highlighting the importance of a detailed knowledge of natural long-term rainfall fluctuations for sustainable socio-economic development.

The partially submerged Crescent Island crater (CIC) basin in Lake Naivasha, Kenya, is unique for equatorial east Africa in combining the climatic sensitivity of a shallow Rift Valley lake with the wind-sheltered sedimentation regime of a deep crater lake⁵. Naivasha is a freshwater lake with subsurface outflow and a short

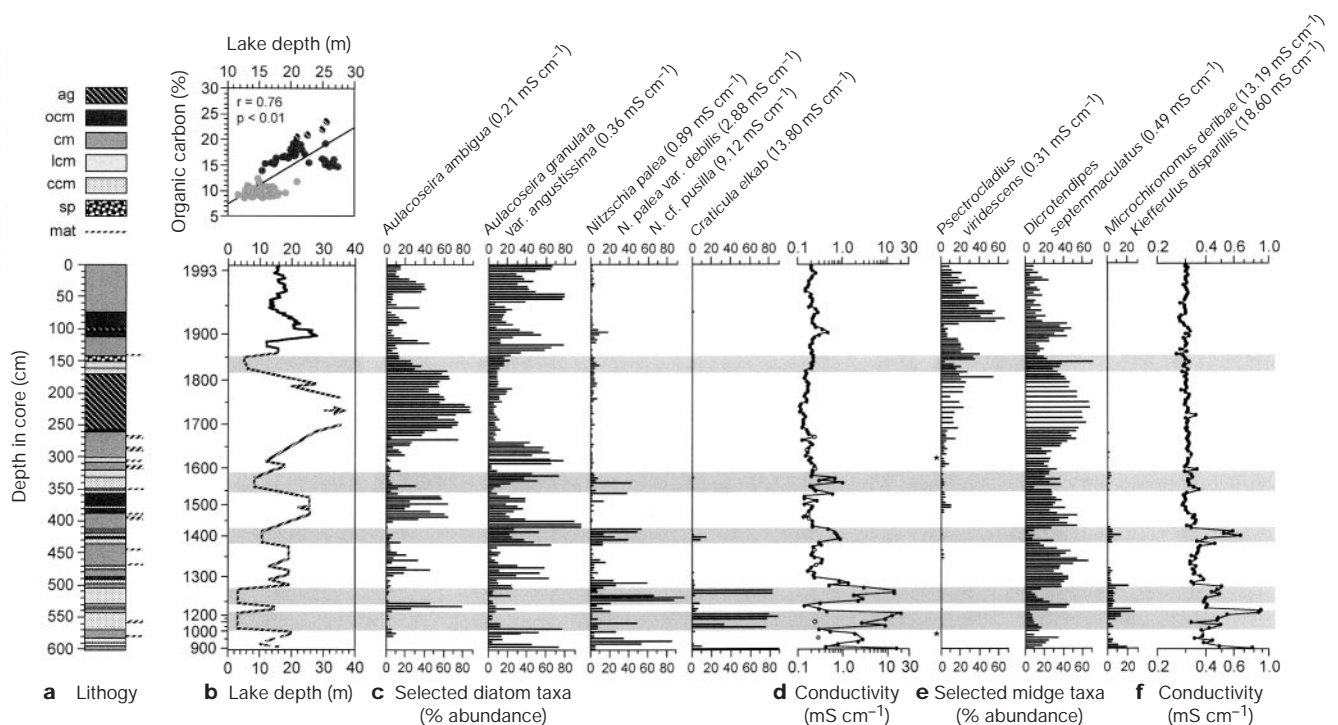


Figure 1 Sedimentological and biological evidence for past lake-depth and salinity fluctuations in the Crescent Island Crater basin of Lake Naivasha. **a**, Stratigraphic distribution of the sediment types algal gyttja (ag), organic clayey mud (ocm), clayey mud (cm), low-organic clayey mud (lcm), calcareous clayey mud (ccm), and silty peat (sp). **b**, Main panel: historical (1883–1993; solid line) and sedimentology-inferred (ref. 8, dashed line) depth variation in relation to sediment age determined by linear interpolation between dated horizons (Table 1). Top, relationship between sedimentary organic carbon and lake depth at the time of deposition in the historical record. **c**, Stratigraphic distribution of selected fossil diatom taxa in 151 horizons at 4-cm intervals (see Supplementary Information for the complete diagram); species labels include the respective salinity optima in reference lakes¹³. **d**, Diatom-inferred conductivity reconstruction; nine data points (open circles) corresponding with dense mono-specific diatom mats ('mat' in **a**) bedded in between sections of the normal sediment matrix are omitted

from the reconstruction because they may represent short-term (<<1 year) events⁸. **e**, Stratigraphic distribution of selected fossil midge taxa in 149 horizons at 4-cm intervals (see Supplementary Information for the complete diagram); stars indicate missing samples, and 18 samples between 192 and 264 cm depth were combined 2-by-2 to improve representability. **f**, Chironomid-inferred conductivity reconstruction. Chironomid- and diatom-inferred conductivity estimates were calculated with weighted-averaging regression and calibration models³¹ based on salinity optima for individual taxa derived from reference data sets of bottom-mud and live diatom floras in 164 African lakes with known water chemistry¹³, and live midge faunas in 45 African lakes with chemistry data compiled from the literature¹¹. Diatom- and chironomid-based conductivity inferences are strongly correlated ($r = 0.64$, $P < 0.01$, $n = 140$), supporting the validity of both proxy salinity indicators.

(< 10 yr) water-residence time⁶, but strong evaporation and highly variable river inflow cause its surface elevation to fluctuate in response to changing climate regimes. Interannual lake-level fluctuation bears the signature of rainfall anomalies linked to El Niño/Southern Oscillation (ENSO) events³, which are regionally complex. At the decadal timescale, remarkably uniform trends in the historical fluctuations of lakes throughout east Africa⁷ indicate that the spatial complexity of rainfall patterns controlled by topography and differences in maritime influence overlays a spatially coherent pattern of temporal variability; this coherent pattern is governed by large-scale atmospheric dynamics of the tropical monsoon circulation³. Since AD 1883 the depth of the CIC basin has ranged between 27 m in AD 1894 and a historic low of 12 m in 1946. The CIC basin functions as a sediment trap for a large sector of Lake Naivasha, resulting in high rates of sediment accumulation and excellent time resolution of its sediment record².

Lake sediments deposited in CIC over the past 1,100 years (Table 1) consist of six types (Fig. 1a, top) which reflect variations in bottom dynamics, clastic input, and water chemistry related to the depth of the lake and its degree of hydrologic closure at the time of deposition⁵. Analyses of modern and historical sedimentation patterns in CIC and neighbouring lakes^{5,8} revealed strong and consistent relationships between sediment composition and lake depth; these relationships can be used to reconstruct former

fluctuations in lake depth from sediment stratigraphy⁸. For example, variation in organic-carbon content in the lithological sequence from clayey mud to gelatinous algal gyttja (Fig. 1a, top) is positively correlated with lake depth (Fig. 1b, top) because its dilution by relatively coarse-grained, inorganic littoral sediments is reduced during highstands⁸. Deposition of calcareous clayey mud reflects biogenic carbonate precipitation following the evaporative concentration of dissolved salts⁹. We interpret its stratigraphic occurrence in CIC sediments (Fig. 1a) to indicate prolonged hydrologic closure of the crater basin during lowstands below the elevation of the sill connecting it to Lake Naivasha. Deposition of silty peat with abundant remains of the aquatic plant *Ceratophyllum* is interpreted to reflect a freshwater lowstand when submerged macrophytes grew across the bottom of the crater (< 5 m depth), while the shallow basin of Lake Naivasha stood dry.

The strong documented relationship between the species distribution of diatoms and the salinity of lakes around the world has yielded regionally robust models for inferring past changes in the salinity of climate-sensitive lakes from fossil diatom assemblages¹⁰. Recent studies on the ecological distribution of aquatic midges of the family Chironomidae (Insecta: Diptera) in lakes of the Kenya Rift Valley^{11,12} suggest that their fossil remains can also provide information on past changes in salinity, as well as lake depth. Here we use a published salinity-inference model based on modern

African diatom floras¹³, and a new model based on modern African chironomid faunas¹¹, to reconstruct decade-scale fluctuations in the conductivity (a common proxy for salinity¹⁰) of CIC water during the past 1,100 years. Together, the sediment-inferred depth reconstruction (Fig. 1b) and diatom- and chironomid-inferred conductivity reconstructions (Fig. 1d,f) show that CIC experienced a long saline lowstand from about AD 1000 to 1270, interrupted by one freshwater interval in the early thirteenth century. This lowstand was followed from ~AD 1270 to 1550 by a mostly positive water balance and establishment of freshwater conditions, except for one recurrence of saline conditions dated to ~AD 1380–1420. After a second pronounced lowstand dated to ~AD 1560–1590, CIC rose to a highstand that lasted from about AD 1670 to 1770, with lake level continuously above the historical maximum reached in 1894. The diatom flora at that time (Fig. 1c; see also Supplementary Information) was dominated by *Aulacoseira ambigua*, consistent with the high light and low nutrient requirements of this species compared to *A. granulata*¹⁴, and the documented influence of lake depth on the light regime and nutrient availability in Lake Naivasha¹⁵. The chironomid fauna (Fig. 1e; see also Supplementary Information) was dominated by *Dicoretendipes septemmaculatus*, consistent with the positive relationship of this species with lake depth in the historical portion of the CIC record ($r = 0.69$, $P < 0.01$, $n = 30$). This relationship results because its preferred habitat of submerged macrophytes^{11,12} expands during highstands into the large bottom areas of Lake Naivasha that slope towards the crater¹⁶. The prominent eighteenth-century highstand ended with strong lake-level decline culminating in a third lowstand during ~AD 1810–1850. In contrast to the earlier lowstands which were saline, CIC maintained freshwater conditions during this most recent drawdown, presumably because the preceding 150 years of broad confluence with the hydrologically open basin of Lake Naivasha had removed its burden of dissolved salts. Renewed lake filling in the mid-nineteenth century achieved the intermediate levels that preceded the historic highstand of the late 1880s and 1890s (Fig. 1b). Pronounced lake-level and salinity fluctuations of CIC over the

past millennium are superimposed on a long-term freshening trend that started around AD 1270; evidence for this freshening is given by the gradual disappearance of salt-tolerant diatom and chironomid taxa (Fig. 1c,e) and the expansion of stenotopic freshwater taxa¹¹ such as *Psectrocladius viridescens* (Fig. 1e).

The combined palaeoenvironmental information we derive from the CIC sediment record describes the hydrological response of Lake Naivasha to a succession of decade-scale fluctuations in the regional balance of rainfall and evaporation over the past 1,100 years. It suggests that equatorial east Africa was generally drier than today during the Mediaeval Warm Period (MWP; ~AD 1000 to 1270), and that fairly wet conditions during the Little Ice Age (LIA; ~AD 1270–1850) were interrupted around AD 1380–1420, 1560–1620 and 1760–1840 by episodes of persistent aridity more severe than any recorded drought of the twentieth century. Previously available proxy climate records from the large African Rift lakes Tanganyika¹⁷ and Turkana¹⁸ lack comparable detail, but are consistent with our inference that tropical east Africa was drier than today during the eleventh and twelfth centuries, and relatively wet from the late thirteenth century to the mid-eighteenth century. Sediment records from shallow lakes in the region are typically incomplete, but a LIA-period highstand of Lake Chilwa in Malawi dated to AD 1650–1760¹⁹ is coeval with the most prominent highstand of Lake Naivasha. The inferred prevalence of drought in tropical Africa during the MWP, and the highest rainfall broadly coincident with the lowest LIA temperatures in mid-latitude regions of the Northern Hemisphere²⁰, implies that the latitudinal pattern of century-scale climate anomalies during the past 1,100 years was opposite to that which occurred on millennial timescales during the last glaciation²¹, the Younger Dryas²², and early Holocene²³.

Comparison of the Naivasha record with that of reconstructed atmospheric ¹⁴CO₂ production, a proposed proxy for long-term changes in solar radiation²⁴, reveals that the MWP period of inferred African aridity and all three severe drought events of the past 700 years were broadly coeval with phases of high solar radiation, and intervening periods of increased moisture were coeval with phases

Table 1 Chronology of the sediment record from Crescent Island Crater basin

Core depth (cm)	Dated horizon or material	²¹⁰ Pb or ¹⁴ C (years AD or BP)	Calendar year AD (1σ range)
Sediment age*			
0	Sediment surface		1993.6
10–11	<i>Salvinia</i> remains		1989
16–17	<i>Salvinia</i> remains		1982
30–31	<i>Salvinia</i> remains		1969
Age of stratigraphic marker horizons†			
49–50	<i>Daphnia</i> resting eggs	1958 ± 4 AD	1958 (1954–1962)
73–74	Transition ocm to cm§	1940 ± 8 AD	1940 (1932–1948)
113–114	Transition cm to ocm§	1890 ± 35 AD	1890 (1855–1925)
Radiocarbon dates‡			
150–178	Grass charcoal	120 ± 50 BP	1819, 1860, 1917 (1803–1937) 1718, 1702 (1680–1753)
350–374	<i>Acacia</i> leaflets, grass charcoal	320 ± 40 BP	1530, 1537, 1635 (1511–1647)
374–398	Grass charcoal	480 ± 50 BP	1436 (1414–1449)
419–420	Sedge rhizome	580 ± 40 BP	1400 (1314–1411)
486–506	<i>Acacia</i> leaflets, grass charcoal	770 ± 50 BP	1278 (1229–1288)
506–510	<i>Acacia</i> twig	(930 ± 50 BP)	1052, 1085, 1121, 1139, 1156 (1028–1178)
538–542	Charred wood	820 ± 50 BP	1229 (1191–1278)
542–546	Wood	(1100 ± 60 BP)	982 (938–1000) 910, 906 (892–930)
558–562	Unburned grass stem	(1250 ± 50 BP)	779 (689–873)
562–566	<i>Acacia</i> wood, leaflet	1030 ± 50 BP	1014 (983–1029)
562–566	Sedge rhizome	1040 ± 50 BP	1011 (978–1026)
592–602	Grass charcoal	1140 ± 60 BP	890 (869–985)

* Sediment age at depth based on fossil evidence of three documented outbreaks of the exotic water fern *Salvinia molesta*.⁵

† Age of stratigraphic marker horizons (years AD ± 1σ) determined by correlation with the equivalent horizons in a ²¹⁰Pb-dated sediment core from the main basin of Lake Naivasha.⁵

‡ Radiocarbon dates (years BP ± 1σ) determined by accelerator mass spectrometry at the Lawrence Livermore National Laboratory. Agreement between the ages of sedge rhizomes and *Acacia* wood retrieved from depth interval 562–566 cm suggests that ¹⁴C dates obtained on emergent aquatic vegetation and terrestrial plant material can be used in combination. Radiocarbon dates were converted to calendar year using the bidecadal calibration curve²⁴, and the continuous sediment chronology was constructed by linear interpolation between these calendar ages. Three out-of-sequence ¹⁴C ages (in parentheses) on single macrofossils recovered from calcareous clayey mud between 506 and 572 cm depth are omitted from the chronology on the basis that they may be derived from older deposits reworked during lowstands⁵. In cases where conversion yielded non-unique calendar ages, a fourth-order polynomial regression of all retained dates was used to determine the relative probability of alternative calendar ages based on minimization of downcore variation in sedimentation rate.

§ Sediment type codes as in Fig. 1.

of low solar radiation (Fig. 2). Hence, variation in solar radiative output may have contributed to decade-scale rainfall variability in equatorial east Africa. Specifically, highest inferred rainfall of the past 1,100 years coincided with the 'Maunder minimum' of solar radiation (AD 1645–1715; ref. 25). The Naivasha record suggests that late-sixteenth-century drought partly preceded peak solar radiation, but the time difference involved is within the uncertainty range of the supporting radiocarbon chronology (Table 1). Similar to historical lake-level records in the region⁷, our 1,100-year reconstruction reflects lake response to decade-scale clusters of years with above- or below-average rainfall, and can thus be considered to reflect the long-term history of water-resource availability in continental east Africa. The amplifying effect of river inflow²⁶ from a large Rift Valley drainage basin allowed the possibly subtle effect of solar forcing on African rainfall to be manifested in Naivasha's lake-level record.

Comparison of this record with the pre-colonial history of east Africa recounted in oral traditions⁴ testifies to the importance of rainfall and drought in agricultural and pastoral societies (Fig. 2). In the six centuries before AD 1895, evidence for drought-induced famine, political unrest, and large-scale migration of indigenous peoples is concentrated in three periods around AD 1390–1420 (Wamara), AD 1560–1625 (Nyarubanga), and AD 1760–1840 (Lapanarat-Mahlatule) that match the reconstructed sequence of Lake Naivasha lowstands (Fig. 2). The intervening 'first and second Age of Prosperity' (ref. 27)—relatively uneventful periods of political stability, consolidation of kingdoms, agricultural success and population growth—are coeval with the two most prominent Lake Naivasha highstands. In the near-complete absence of archeological data²⁸, the Lake Naivasha record establishes the environmental background for political and cultural change in pre-colonial east Africa, indicates strong links between cultural development and

climate change, and reinforces the chronology of historical events as derived from oral traditions.

Lack of long palaeomoisture records from low-latitude regions has thus far limited our understanding of global climate variability at decade-to-century timescales¹, and hindered efforts to identify physical feedback mechanisms that may strengthen the direct temperature effect of long-term changes in solar radiation²⁹. Our results corroborate findings from north-temperate dryland regions³⁰ that instrumental climate records are inadequate to appreciate the full range of natural variation in drought intensity at timescales relevant to socio-economic activity. The magnitude of natural decade-scale rainfall variability in sub-humid east Africa implies that sustainable development and protection of food security will require agricultural management strategies adjusted to major long-term variation in water-resource availability, irrespective of any future effects of anthropogenic climate change on the hydrological cycle. □

Received 8 April; accepted 16 November 1999.

1. Houghton, J. T. et al. (eds). *Climate Change 1995 The Science of Climate Change* (Cambridge Univ. Press, 1995).
2. Nicholson, S. E. *The Physical Geography of Africa* (eds Goudie, A. S., Adams, W. M. & Orme A.) 60–75 (Oxford Univ. Press, 1995).
3. Nicholson, S. E. in *The Limnology, Climatology and Paleoclimatology of the East African Lakes* (eds Johnson, T. C. & Odada, E.) 25–56 (Gordon & Breach, Newark, 1996).
4. Webster, J. B. in *Chronology, Migration and Drought in Interlacustrine Africa* (ed. Webster J. B.) 1–37 (Longman & Dalhousie Univ. Press, Dalhousie, 1979).
5. Verschuren, D. Sedimentation controls on the preservation and time resolution of climate-proxy records from fluctuating lakes. *Quat. Sci. Rev.* **18**, 821–837 (1999).
6. Ojiambo, B. S. & Lyons, W. B. in *The Limnology, Climatology and Paleoclimatology of the East African Lakes* (eds Johnson, T. C. & Odada, E.) 267–278 (Gordon & Breach, Newark, 1996).
7. Nicholson, S. E. in *Environmental Change and Response in East African Lakes* (ed. Lehman J. T.) 7–35 (Kluwer, Dordrecht, 1998).
8. Verschuren, D. Reconstructing fluctuations of a shallow East African lake during the past 1800 years from sediment stratigraphy in a submerged crater basin. *J. Paleolimnol.* (in the press).
9. Kilham, P. Mechanisms controlling the chemical composition of lakes and rivers: data from Africa. *Limnol. Oceanogr.* **35**, 80–83 (1990).
10. Fritz, S. C., Cumming, B. F., Gasse, F. & Laird, K. R. in *Diatoms: Applications to the Environmental and Earth Sciences* (eds Stoermer, E. & Smol, J. P.) 41–72 (Cambridge Univ. Press, 1999).
11. Verschuren, D. Taxonomy and ecology of fossil Chironomidae (Insecta, Diptera) from Rift Valley lakes in central Kenya. *Arch. Hydrobiol. Suppl.* **107**, 467–512 (1997).
12. Verschuren, D., Tibby, J., Sabbe, K. & Roberts, N. Effects of lake level, salinity and substrate on the benthic invertebrate community of a shallow tropical-African lake ecosystem. *Ecology* (in the press).
13. Gasse, F., Juggins, S. & Ben Khelifa, L. Diatom-based transfer functions for inferring hydrochemical characteristics of African paleolakes. *Palaeoecol. Palaeoecol.* **117**, 31–54 (1995).
14. Kilham, P., Kilham, S. S. & Hecky, R. E. Hypothesized resource relationships among African planktonic diatoms. *Limnol. Oceanogr.* **31**, 1169–1181 (1986).
15. Harper, D. M., Phillips, G., Chilvers, A., Kitaka, N. & Mavuti, K. Eutrophication prognosis for Lake Naivasha, Kenya. *Verh. Int. Verein. Limnol.* **25**, 861–865 (1993).
16. Harper, D. M. The ecological relationships of aquatic plants at Lake Naivasha, Kenya. *Hydrobiologia* **232**, 65–71 (1992).
17. Cohen, A. S., Talbot, M. R., Awramik, S. M., Dettman, D. L. & Abell, P. Lake level and paleoenvironmental history of Lake Tanganyika, Africa, as inferred from late Holocene and modern stromatolites. *Geol. Soc. Am. Bull.* **109**, 444–460 (1997).
18. Halfman, J. D., Johnson, T. C. & Finney, B. P. New AMS dates, stratigraphic correlations and decadal climatic cycles for the past 4 ka at Lake Turkana, Kenya. *Palaeoecol. Palaeoecol.* **111**, 83–98 (1994).
19. Owen, R. B. & Crossley, R. Recent sedimentation in lakes Chilwa and Chiuta, Malawi. *Palaeoecol. Afr.* **20**, 109–117 (1989).
20. Mann M. E., Bradley, R. S. & Hughes, M. K. Northern hemisphere temperatures during the past millennium: inferences, uncertainties, and limitations. *Geophys. Res. Lett.* **26**, 759–762 (1999).
21. Kutzbach, J. E. & Street-Perrott, F. A. Milankovitch forcing of fluctuations in the level of tropical lakes from 18 to 0 kyr BP. *Nature* **317**, 130–134 (1985).
22. Roberts, C. N. et al. Timing of the Younger Dryas event in East Africa from lake-level changes. *Nature* **366**, 146–148 (1993).
23. Street-Perrott, F. A. & Perrott, R. A. Abrupt climate fluctuations in the tropics: the influence of Atlantic Ocean circulation. *Nature* **348**, 607–612 (1990).
24. Stuiver, M. & Reimer, P. J. Extended ¹⁴C data base and revised CALIB 3.0 ¹⁴C age calibration program. *Radiocarbon* **35**, 215–230 (1993).
25. Lean, J., Beer, J. & Bradley, R. S. Reconstruction of solar irradiance since 1610: implications for climate change. *Geophys. Res. Lett.* **22**, 3195–3198 (1995).
26. Knox, J. C. Large increases in flood magnitude in response to modest changes in climate. *Nature* **361**, 430–432 (1993).
27. Webster, J. B. Drought, migration and chronology in the Lake Malawi littoral. *Transafr. J. Hist.* **9**, 70–90 (1980).
28. Connah, G. *African Civilizations* (Cambridge Univ. Press, 1987).
29. Rind, D. & Overpeck, J. Hypothesized causes of decade-to-century-scale climate variability: climate model results. *Quat. Sci. Rev.* **12**, 357–374 (1993).
30. Woodhouse, C. A. & Overpeck, J. T. 2000 years of drought variability in the central United States. *Bull. Am. Meteorol. Soc.* **79**, 2693–2714 (1998).

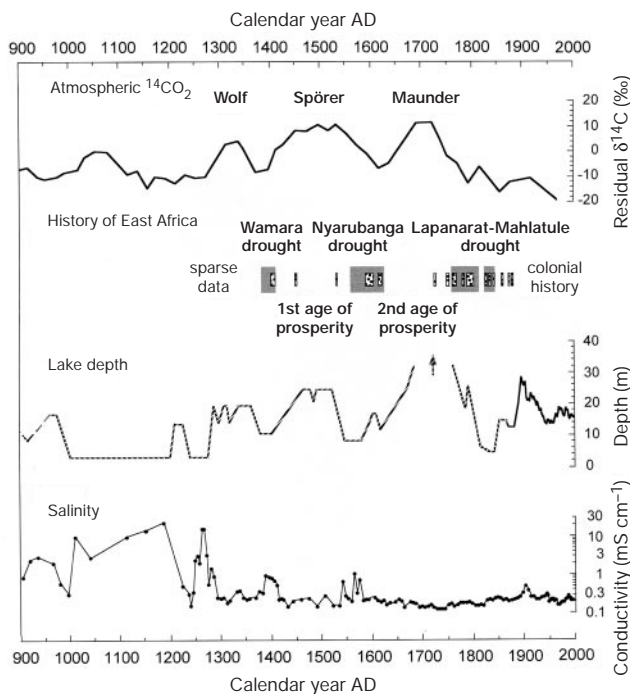


Figure 2 Comparison of Crescent Island Crater history with documented and reconstructed climate-proxy data. Shown is a comparison of reconstructions of the depth and salinity of Crescent Island Crater lake with the decadal record of atmospheric ¹⁴CO₂ production²⁴ as a proxy for solar radiation, and the pre-colonial history of east Africa. Grey bars indicate evidence of drought-related political upheaval recorded in oral tradition, genealogically dated using a 27-yr dynastic generation⁴. Stippled bars compile the evidence of severe drought events from various archival records² including the (incomplete) record of Nile River discharge.

31. Line, J. M., ter Braak, C. J. F. & Birks, H. J. B. WACALIB version 3. 3: A computer program to reconstruct environmental variables from fossil assemblages by weighted averaging and to derive sample-specific errors of prediction. *J. Paleolimnol.* **10**, 147–152 (1994).

Supplementary information is available on Nature's World-Wide web site (<http://www.nature.com>) or as paper copy from the London editorial office of Nature.

Acknowledgements

We thank K. Mavuti, B. Ammann, F. Janssen and H. E. Wright for field assistance; the Lake Naivasha Riparian Association for lake access; F. Gasse for use of the African diatom reference and calibration data sets; and S. Fritz, F. Gasse, K. Kelts, F. Oldfield, J. P. Smol, B. Tinsley and H. E. Wright for comments on the manuscript. This work was supported by NSF, the Quaternary Paleocology Program at the University of Minnesota, and by fellowships from NOAA and FWO-Vlaanderen (D.V.) The fieldwork was conducted with permission from the Office of the President of the Republic of Kenya to K. Mavuti.

Correspondence should be addressed to D.V. (e-mail: dirk.verschuren@rug.ac.be). The data presented here are archived at the World Data Center-A for Paleoclimatology.

Precise climate monitoring using complementary satellite data sets

Frank J. Wentz & Matthias Schabel

Remote Sensing Systems, 438 First Street, Suite 200, Santa Rosa, California 95401, USA

Observations from Earth-orbiting satellites have been a key component in monitoring climate change for the past two decades. This has become possible with the availability of air temperatures from the Microwave Sounding Unit (MSU)¹ since 1979, sea surface temperatures from the Advanced Very High Resolution Radiometer (AVHRR)² since 1982 and, most recently, measurements of atmospheric water vapour content from the Special Sensor Microwave Imager (SSM/I)³ since 1987. Here we present a detailed comparison of each pair of these three time series, focusing on both interannual and decadal variations in climate. We find a strong association between sea surface temperature, lower-tropospheric air temperature and total column water-vapour content over large oceanic regions on both time scales. This lends observational support to the idea of a constant relative humidity model having a moist adiabatic lapse rate. On the decadal timescale, the combination of data sets shows a consistent warming and moistening trend of the marine atmosphere for 1987–1998.

The detection and measurement of small changes in the Earth's climate require extremely precise global observations of a broad spectrum of complementary physical variables. In this endeavour, satellite observations are playing an increasingly important role. As compared to conventional *in situ* observations, satellites provide daily near-global coverage with a very high statistical precision that results from averaging millions of individual observations. Here we present a three-way intercomparison of three satellite-derived climate variables that are closely correlated in the marine boundary layer and lower troposphere: sea surface temperature T_S , lower-tropospheric air temperature T_A , and vertically integrated, or columnar, atmospheric water vapour W . This intercomparison allows us to determine the coupling of the three variables on interannual and decadal timescales and investigate the accuracy of the individual time series^{4,5,6}.

The T_A and T_S data sets are standard products that have been available for some time^{1,2}, whereas the W data set is a relatively new product³ beginning in 1987 with the launch of the special sensor microwave imager (SSM/I), a multichannel microwave radiometer.

Since 1987 four more SSM/Is have been launched, providing an uninterrupted 12-year time series. Imaging radiometers before SSM/I were poorly calibrated, and as a result early water-vapour studies⁷ were unable to address climate variability on interannual and decadal timescales.

To retrieve water vapour from the SSM/I observations, we use a physically based algorithm that simultaneously computes water vapour, wind speed, and cloud water by directly matching the observations to a radiative transfer model³. The primary channel for W is at 22 GHz, which is centred on a water-vapour absorption line. Additional dual-polarization channels at 19 and 37 GHz are used to remove crosstalk (that is, a signal from one variable aliasing into another) attributable to wind and clouds. A monthly climatology is used to specify the regional and seasonal variations of T_S . The T_A and T_S decadal time series are used to remove a small crosstalk component on interannual timescales. This correction for interannual crosstalk is quite small, reducing the amplitude of the interannual variability in W by about 8%. Other water-vapour retrieval algorithms have been developed, but most do not fully account for crosstalk or do not use the 22-GHz channel^{8,9}, thereby limiting their ability to measure the small interannual climate signal. The retrieval of W requires the radiometrically cold background of the sea surface and cannot be done over land, which is highly emissive.

For the intercomparisons, we use Reynolds' 1982–1998 optimally interpolated sea surface temperature data set² and the 1979–1998 version-c1 MSU lower-tropospheric air temperature¹⁰ with a correction for orbital decay that is added to the zonal averages⁶. (We do not use the new version-d MSU product because it has not yet been published. However, for the intercomparison period (1987–1998) over the oceans, there is little difference (0.01 K per decade) between version c1 plus orbit decay and version d.) The three variables are geographically and temporally sampled in the same manner to ensure an unbiased comparison. Figure 1 shows the deseasonalized anomalies of W , T_S , and T_A . Results are shown for three zones: the northern extratropics (20°N–60°N), the tropics (20°N–20°S), and the southern extratropics (20°S–60°S). The seasonal cycle has been removed and the residuals have been low-pass filtered by convolution with a gaussian distribution having a ± 90 -day width at half-peak value. The variation of water vapour with latitude is large (5–60 mm), so it is more convenient to express W in terms of a percentage change. To compute percentages, the daily zonal W is divided by the 12-year mean value for the zone. The prominent El Niño/Southern Oscillation signal is clearly evident in the tropics, peaking in January 1983, December 1987 and December 1997. For the 1983 and 1997 El Niños, the T_S signal leads T_A by a few months, but the 1987 El Niño shows no such lag. The scaling in Fig. 1 is based on radiosonde observations of mid-latitude seasonal variability, which show $\Delta W/\Delta T_S = 11\% \text{ K}^{-1}$ and $\Delta T_A/\Delta T_S = 1.6$. To display this scaling, the T_A time series have been divided by 1.6, and the vapour scale on the right side of the figure is chosen so that $11\% = 1 \text{ K}$.

Three statistics for the 1987–1998 period are given in Table 1: the correlation coefficient, the decadal trend, and the scaling coefficient, which is the ratio of standard deviations of the time series. The three variables are closely coupled, as has been shown by previous studies on shorter timescales of 2–5 years (refs 9 and 11). In the tropics, where the El Niño/Southern Oscillation cycle dominates the interannual variability, the correlation coefficients are very high: W with T_S is 0.98, W with T_A is 0.93, and T_S with T_A is 0.94. The corresponding tropical scaling coefficients are $\Delta W/\Delta T_S = 9.2\% \text{ K}^{-1}$, $\Delta T_A/\Delta T_S = 1.4$ and $\Delta W/\Delta T_A = 6.7\% \text{ K}^{-1}$, which are similar to the mid-latitude radiosonde seasonal scalings. These tropical scaling relationships are consistent with a constant relative humidity (H_{rel}) model having a moist adiabatic lapse rate (MALR)¹². The Clausius–Clapeyron equation for saturation vapour pressure¹³ predicts that the water-vapour density, and hence columnar content, increases

